

# Study on magnetization dynamics modulated by spin-orbit-torque in a $\text{Ni}_{81}\text{Fe}_{19}/\text{NiO}/\text{Ni}_{81}\text{Fe}_{19}$ multilayered wire

Cite as: AIP Advances **13**, 025341 (2023); <https://doi.org/10.1063/9.0000397>

Submitted: 29 September 2022 • Accepted: 15 January 2023 • Published Online: 08 February 2023

 Akinobu Yamaguchi, Nobuko Matsumoto, Wataru Yoshikawa, et al.

## COLLECTIONS

Paper published as part of the special topic on [67th Annual Conference on Magnetism and Magnetic Materials](#)



View Online



Export Citation



CrossMark



# Study on magnetization dynamics modulated by spin-orbit-torque in a $\text{Ni}_{81}\text{Fe}_{19}/\text{NiO}/\text{Ni}_{81}\text{Fe}_{19}$ multilayered wire

Cite as: AIP Advances 13, 025341 (2023); doi: 10.1063/9.0000397

Submitted: 29 September 2022 • Accepted: 15 January 2023 •

Published Online: 8 February 2023



View Online



Export Citation



CrossMark

Akinobu Yamaguchi,<sup>1,a)</sup>  Nobuko Matsumoto,<sup>2</sup> Wataru Yoshikawa,<sup>2</sup> and Yasuhisa Fujii<sup>2</sup>

## AFFILIATIONS

<sup>1</sup> LASTI, University, Hyogo 3-1-2 Kouto, Kamigori, Hyogo 678-1205, Japan

<sup>2</sup> KRI Inc., 134, Chudoujiminamimachi, Chudouji, Kyoto 600-8813, Japan

**Note:** This paper was presented at the 67th Annual Conference on Magnetism and Magnetic Materials.

**a) Author to whom correspondence should be addressed:** [yamaguti@lasti.u-hyogo.ac.jp](mailto:yamaguti@lasti.u-hyogo.ac.jp). Telephone: +81-791-58-0041

## ABSTRACT

As electrical control of magnetization dynamics opens the door to realize spintronic devices, understanding the microscopic mechanisms of spin current transport and its effect through the antiferromagnetic and interface is crucial. We studied magnetization dynamics modulated by the spin current originated from the spin-orbit-torque using the rectifying planar Hall effect (PHE). In  $\text{Ni}_{81}\text{Fe}_{19}/\text{NiO}/\text{Ni}_{81}\text{Fe}_{19}$  heterostructure wire deposited on Pt/Ta cross-tie electrode, we measured the rectifying PHE as a function of external magnetic field angle and dc electric current. By measuring the electrical responses of the heterostructure system, we found that the magnetization dynamics can be modulated by the dc electric current flowing through the Pt/Ta electrode.

© 2023 Author(s). All article content, except where otherwise noted, is licensed under a Creative Commons Attribution (CC BY) license (<http://creativecommons.org/licenses/by/4.0/>). <https://doi.org/10.1063/9.0000397>

## I. INTRODUCTION

Manipulation of magnetic properties and its dynamics in magnetic thin films have attracted a great deal of attention in various research and development fields because of their unique properties.<sup>1–3</sup> Spin transfer torque (STT) is often used to write the magnetic state.<sup>4–14</sup> The STT is a torque derived from the spin angular momentum transition, enabling magnetization reversal to be realized by electric current. That is memory writing or switching can be realized by the STT. In addition, the STT-based devices can also become not only the microwave detection devices but oscillator.<sup>15–20</sup> However, in order to generate the STT that realizes magnetization reversal, a large current density is required for the magnetization reversal. This intrinsic principle indicates that there are problems in device reliability, limitation for number of writes, and power saving.

Recently, a new type of spin dynamics excitation method based on current-induced spin orbit torques (SOT) in a  $\text{Pt(permalloy)}/\text{Pt(platinum)}$  bilayer was demonstrated.<sup>21</sup> This SOT

is derived from the interface effect associating with ferromagnetic and non-magnetic heavy metallic layers, that is the SOT in this system can be induced from the spin Hall effect in Pt and the Rashba effect at the interface between  $\text{Pt}$  and  $\text{Pt}$  layers.<sup>21–30</sup> While the STT element described above directly inputs a current to a magnetic tunnel junction (MTJ) or a domain wall, an electric current is passed through the element electrode in the SOT-based devices. That is in the STT element, since the current flows directly through the MTJ, the energy efficiency is good, but there is a possibility of breaking the MTJ due to the leakage current. If an electric current that does not flow directly to the element can be used, the reliability of the MTJ can be ensured. In addition, by using SOT, there is a possibility that the current density required for magnetization reversal can be reduced. This discovery and application of SOT paved the way for the practical application of SOT-based magnetic random-access memory (MRAM).

In recent years, the antiferromagnets (AFMs) and multilayers combining with ferromagnets (FMs) and AFMs have been focused because these systems show a low magnetic susceptibility and

terahertz (THz) spin dynamics.<sup>31,32</sup> By increasing the wireless communication frequency, it is expected that the next generation sixth generation (6G) communication frequency band in the THz region, and it is attracting more attention. Recently, in the studies associated with the spin dynamics and spin transport properties, FM/AFM/heavy metal trilayer structures have been often used to investigate spin transport in insulating AFMs. Experimental techniques include the following two methods: one is microwave-filed-induced magnetization dynamics in the FM layer to generate a spin current transmitted through the AFM layer, the other is spin Hall magnetoresistance measurements. These experimental studies have indicated that the NiO layer can be an efficient spin conductor by evanescent spin wave propagation. Shang *et al.* suggested that NiO can suppress the magnetic proximity effect and have possibility to conduct spin transport between Pt and yttrium iron garnet (YIG) through NiO layers.<sup>33</sup>

Here, we focused on the structure of the multilayer film and demonstrated systematically measuring its spin dynamics and spin Hall magnetoresistance. If NiO layer suppresses the magnetic proximity effect and couples with the evanescent spin waves as described above, quantum interference based on the spin waves should be induced through the AFM. In recent years, several methods have been proposed for the quantitative evaluation of SOT. One is the harmonic Hall voltage measurement method, which is a kind of electrical torque measurement,<sup>34–38</sup> the other is the planar Hall effect (PHE) measurement method by rectifying ferromagnetic resonance.<sup>38–43</sup> The former is a method of evaluating from a relatively static response characteristic, and the latter is a method of evaluating from a dynamic response. In this study, we demonstrated the modulation of magnetization dynamics in the multilayer structure consisting of  $\text{Ni}_{81}\text{Fe}_{19}/\text{NiO}/\text{Ni}_{81}\text{Fe}_{19}$  by the SOT via the observation based on the rectifying PHE.

## II. SAMPLE PREPARATIONS AND EXPERIMENTAL METHODS

Using electron-beam lithography and a lift-off process, we fabricated systems comprising Substrate ( $\text{SiO}_2/\text{Si}$ )/Ta(2 nm)/Pt(10 nm) electrode/ $\text{Ni}_{81}\text{Fe}_{19}$  (25 nm)/NiO (3 nm)/ $\text{Ni}_{81}\text{Fe}_{19}$  (5 nm). The sample line was  $5\ \mu\text{m}$  in width and  $100\ \mu\text{m}$  in length. In lift-off process, using a magnetron sputtering machine, thin films were deposited onto a  $\text{SiO}_2/\text{Si}$  substrate at room temperature. For simultaneous measurements of magnetoresistance (MR) and PHE voltage of a system, a cross-shaped electrode consisting of Ta/Pt was prepared as schematically illustrated in Fig. 1. The width and thickness of the electrode are  $10\ \mu\text{m}$  and 60 nm, respectively. After the preparation of the cross-shaped electrode, the trilayer wire was formed on the electrode. Finally, the coplanar waveguide electrode was fabricated. To measure the electromagnetic properties, a ground-signal-ground (GSG)-type microwave probe was connected to the gold electrode, as schematically illustrated in Fig. 1(a).<sup>38,39</sup> The optical micrograph of the prepared device is displayed in Fig. 1(b). We prepared a home-made automatic rotating magnetic field application system as schematically illustrated in Fig. 1(c). This field application system can freely rotate  $360^\circ$  and apply an external magnetic field up to about 200 G. For microwaves, up to 40 GHz can be used. We placed the device onto the system as shown in Fig. 1(d). Using the system, we evaluate the simultaneous rectifying voltage

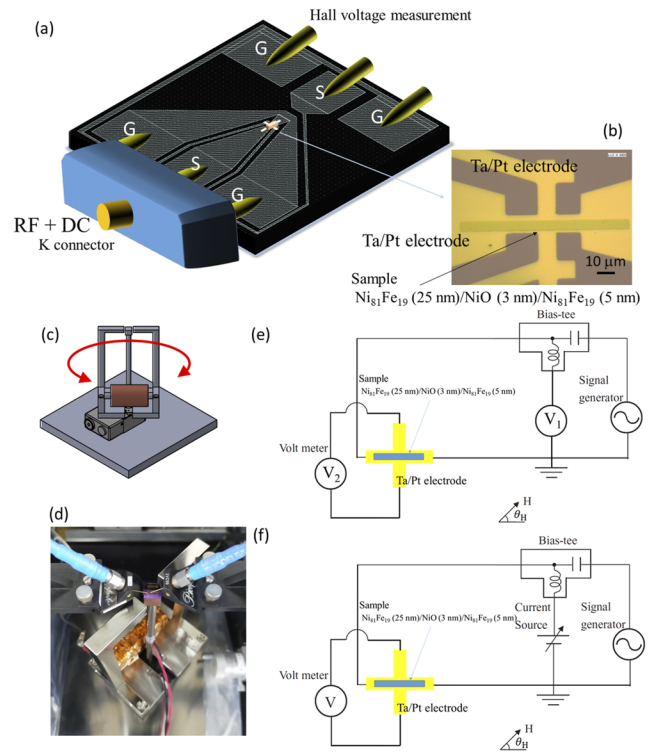


**FIG. 1.** (a) Schematic of the sample geometry including Ground-Signal-Ground (GSG) microwave probes for Radio frequency (RF) + direct current (DC) inputs and Planar Hall voltage measurements. (b) An optical image of the sample. (c) Schematic of home-made automatic angle rotation measurement system. (d) An optical image of the measurement system. Schematics of the electrical measurement circuits for the rectifying spectra (e) without and (f) with the DC electric current, respectively. The external static magnetic field,  $H_{\text{ext}}$ , is applied in the substrate plane at the angle of  $\theta_H$  from the longitudinal axis of the wire.

spectra from the long-axis and short-axis directions of the wire using an electric circuit drawn in Fig. 1(e). Magnetization dynamics induced by the application of dc current was measured through the rectifying PHE using the electric circuit schematically illustrated in Fig. 1(f). A coordinate system is defined as schematically illustrated in Figs. 1(e) and 1(f). The direction parallel to the long-axis of the wire is defined as  $\theta = 0^\circ$  for the magnetic field application angle. All measurements were performed at room temperature.

## III. PHENOMENOLOGICAL CALCULATION FOR MAGNETIZATION DYNAMICS BASED ON MACRO-SPIN MODEL

The electric transport in a ferromagnet generally depends on the direction of the magnetization. In this case, most of the electric current flows through the Pt electrode, but a part of electric current flows the magnetic multilayer. The system consisting of multilayer on Pt electrode can be described by an equivalent circuit, and can be regarded as an element in which a resistor including a magnetic materials, an inductor component, and a capacitor component are

combined. The phenomenological relationship between the electric field  $\mathbf{E}$  and the electrical current density  $\mathbf{j}$  is written as<sup>3,38–41</sup>

$$\mathbf{E} = \rho_{\perp} \mathbf{j} + \mathbf{m}(\mathbf{j} \cdot \mathbf{m}) \cdot (\rho_{\parallel} - \rho_{\perp}) + \rho_H \mathbf{m} \times \mathbf{j}, \quad (1)$$

where  $\mathbf{m}$  is the unit vector along the local magnetization,  $\rho_{\perp}$  and  $\rho_{\parallel}$  are the resistivities perpendicular and parallel to  $\mathbf{j}$ , respectively, and  $\rho_H$  is the extraordinary Hall resistivity. Assuming that the magnetization oscillates in time, an oscillating component of the magnetization  $\mathbf{m} = \mathbf{m}_0 + \delta\mathbf{m}(t)$  can be introduced into Eq. (1). Here, the magnetization dynamics can be described by the following Landau–Lifshitz–Gilbert equation including the spin torque:<sup>4–8</sup>

$$\frac{d\mathbf{m}}{dt} = -\gamma \mathbf{m} \times \mathbf{B}_S + \frac{\alpha}{M_S} \mathbf{m} \times \frac{d\mathbf{m}}{dt} + \mathbf{T}_{DL} + \mathbf{T}_{FL}, \quad (2)$$

where  $\alpha$  is the damping factor,  $\mathbf{B}_S$  is the effective field,  $\gamma$  is the effective gyromagnetic ratio, and  $M_S$  is the saturation magnetization.  $\mathbf{T}_{DL}$  and  $\mathbf{T}_{FL}$  denote the damping-like (DL) and field-like (FL) torques, respectively. The details of the calculation are left to the literature, and the resulting spectral function can be described as follows. Using the macro-spin model as the first approximation, the rectifying voltage spectrum fitting function of rf frequency,  $f$ , is given by

$$F(f) = A + B \cdot f + C \cdot \frac{1}{(f_r^2 - f^2)^2 + (\Delta f \cdot f)^2} + D \cdot \frac{(f_r^2 - f^2)}{(f_r^2 - f^2)^2 + (\Delta f \cdot f)^2}. \quad (3)$$

Here,  $A$ ,  $B$ ,  $C$ , and  $D$  are fitting parameters.  $A$  and  $B$  are the background contributions.  $C$  and  $D$  correspond to the coefficients derived from the symmetric Lorentz-like and asymmetric dispersive-like terms, respectively. The spectrum can be described with the same shape regardless of the origins such as PHE and AMR. Here, the ferromagnetic resonance frequency,  $f_r$ , is given by

$$f_r = \frac{\gamma}{2\pi} \sqrt{H_{\text{eff}}^{\perp} H_{\text{eff}}^{\parallel}}, \quad (4)$$

where  $\gamma/2\pi = 3.52 \times 10^4$  Hz/(A/m) is the gyromagnetic ratio. An external magnetic field  $H_{\text{ext}}$  is applied at an angle  $\theta_H$  from the

easy axis in the plane. The terms  $H_{\text{eff}}^{\perp}$  and  $H_{\text{eff}}^{\parallel}$  denote the effective in-plane and out-of-plane magnetic anisotropy fields, respectively, given by<sup>38,39</sup>

$$H_{\text{eff}}^{\perp} = H_{\text{ext}} \cos(\theta_H - \theta_M) + \frac{M_S}{\mu_0} (N_y - N_x) \cos 2\theta_M + J_{\text{ex}} \cos(\theta_j - \theta_M) \quad (5)$$

And

$$H_{\text{eff}}^{\parallel} = H_{\text{ext}} \cos(\theta_H - \theta_M) + \frac{M_S}{\mu_0} \{N_z - (N_x \cos^2 \theta_M + N_y \sin^2 \theta_M)\} + J_{\text{ex}} \cos(\theta_j - \theta_M), \quad (6)$$

where  $M_S$  is the saturation magnetization and  $N_{\alpha}$  ( $\alpha = x, y, z$ ) is a demagnetizing factor in the Cartesian coordinate system  $(x, y, z)$ . In addition, we added an effective field,  $J_{\text{ex}}$ , associated with the contribution from the heterojunction.  $J_{\text{ex}}$  is originated from the heterojunction effect including magnetostrictive effect, magnetoelastic effect, Rashba interaction and Dzyaloshinskii–Moriya interaction,<sup>44,45</sup> etc. When spin torque acts, the resonance frequency and full width at half maximum (FWHM) are modulated as follows:  $f_r = \frac{\gamma}{2\pi} \sqrt{H_{\text{eff}}^{\perp} H_{\text{eff}}^{\parallel} + T_{ST}^2}$  and  $\Delta = \alpha (H_{\text{eff}}^{\perp} + H_{\text{eff}}^{\parallel}) + 2T_{ST}$ , where  $T_{ST}$  (associating with  $\mathbf{T}_{DL}$  and  $\mathbf{T}_{FL}$ )  $\propto \mathbf{j}$ , respectively.

#### IV. RESULTS AND DISCUSSIONS

Figures 2(a) and 2(b) show typical spectra obtained from the parallel and perpendicular directions to the rf current flowing direction in the absence of dc current, respectively. The external magnetic field application angle was set at  $\theta_H = 15^\circ$ . In both cases, the resonance structures are clearly observed. Both resonance frequencies are consistent with each other. The resonance voltage amplitude was defined as the peak-to-peak voltage. Here, we define respective voltage amplitudes at the resonance frequency as  $V_1$  and  $V_2$ , as shown in Figs. 2(a) and 2(b). The signal,  $V_1$ , is due to the oscillation of anisotropic magnetoresistive effect (AMR). On the other hand, the signal,  $V_2$ , is derived from the oscillation of PHE. Next, the angle dependences of the resonance voltage amplitude are shown in Figs. 3(a) and 3(b). It was found that  $V_1$  and  $V_2$  show the external magnetic field dependence of the curves of  $\sin 2\theta_H \cos \theta_H$  and  $\cos 2\theta_H \cos \theta_H$ , respectively. The measured angle dependences are

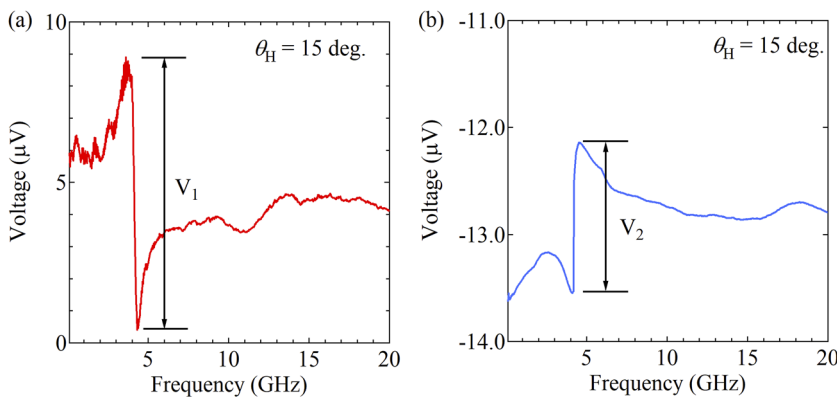


**FIG. 2.** The typical dc voltage spectra for (a) the longitudinal and (b) Hall directions at  $\theta_H = 15^\circ$ , respectively. The (a) red and (b) blue curves correspond to the spectra originated from the anisotropic magnetoresistance (AMR) and planar Hall effect (PHE), respectively.

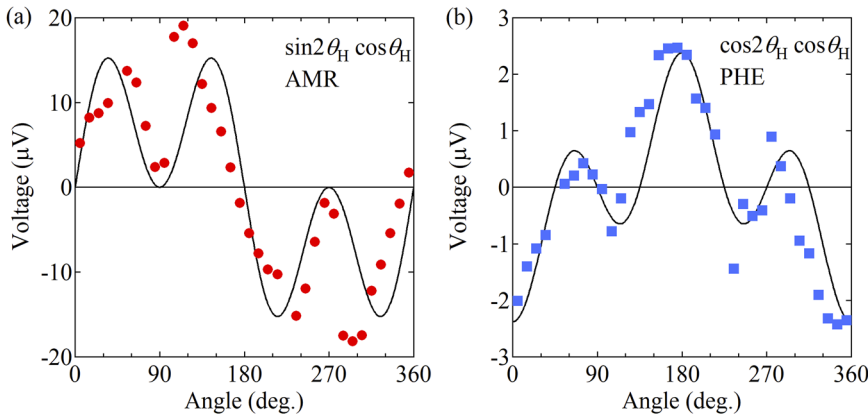


**FIG. 3.** The magnetic field angle  $\theta_H$  dependence of the dc voltage differences (a)  $V_1$  and (b)  $V_2$  at the FMR frequency. The red circles and blue squares are measured data. The black solid curves denote the fittings curves proportional to  $\sin 2\theta_H \cos \theta_H$  and  $\cos 2\theta_H \cos \theta_H$ .

in good agreement with the fitting results anticipated from the macro-spin dynamics model. That is it can be understood that the magnetization dynamics are excited in a state close to a single magnetic domain structure, and each rectified spectrum is expressed through the AMR oscillation. As a result, it can be expected that PHE can be used to investigate the contribution or impact of SOT.

Figure 4 shows the  $\theta_H$  dependence of resonance frequency. The fitting with Eq. almost follows the measured data. This also indicates that the magnetization precession is obeyed by the single macro-spin model. The small discrepancy between the experimental and theoretical results in the  $\theta_H$  dependence of resonance frequency is considered to be caused by the inhomogeneity of the magnetization at the edges of the wire. These fitting curves shown in Figs. 3 and 4 are in good agreement with the experimental results. Their experimental results can be adequately explained in terms of phenomenological analytical macro-spin model.

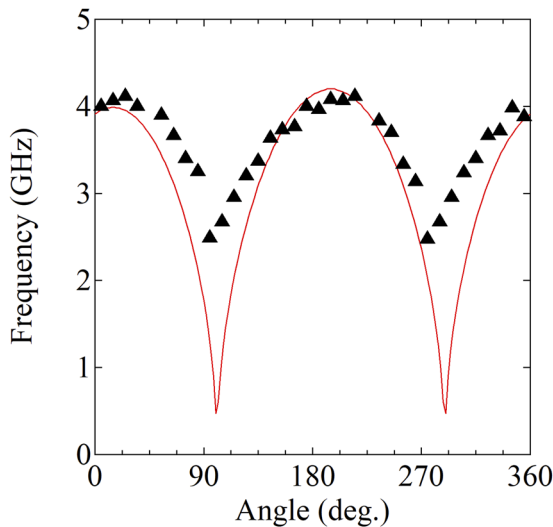


**FIG. 4.** FMR frequency as a function of the applied field angle  $\theta_H$ . The red solid line represents the corresponding fit with Eq. (3).

Next, in order to investigate the contribution of SOT, it is necessary to detect and analyze the spin dynamics while applying a direct current (dc) electric current along the long axis direction of the thin wire. Using the electric circuit shown in Fig. 1(f), the rectifying PHE voltage spectra were measured. When a dc power supply was connected to the bias-T and dc electric current is applied directly to the cross-type Pt electrode, FL-spin torque due to SOT is expected to be induced through the hetero-interface between ferromagnet and Pt electrode. In the strong exchange limit, when the electric field,  $E$ , is applied to the  $x$ -direction, microscopic calculations describe that the FL-spin torque,  $T_{FL} \propto m \times (z \times E)$ , where  $z$  is the unit vector along the  $z$ -direction, due to SOT is expressed as<sup>46</sup>

$$T_{FL} \sim -2e\alpha_R v_0 \left( \frac{\varepsilon_F + J_{ex}}{\gamma_{\uparrow}} - \frac{\varepsilon_F - J_{ex}}{\gamma_{\downarrow}} \right) m \times (z \times E), \quad (7)$$

where  $e$ ,  $\alpha_R$ ,  $v_0$ ,  $\varepsilon_F$ ,  $\gamma_{\uparrow(\downarrow)}$ , and  $J_{ex}$  are the electron charge, Rashba SOI strength at the interface, density of states per spin for two dimensional electron gas, the Fermi energy, and strength of the spin-dependent disorder scattering, and  $sd$  exchange interaction strength, respectively. The FL-SOT spin torque,  $T_{FL}$ , is originated from the scattering of spin carries at the Ferumi surface with a conductivity like behavior. The DL-SOT spin torque,  $T_{DL}$ , is given by  $T_{DL} \propto m \times T_{FL}$ , with an intrinsic nature arising from the Berry phase curvature in the bang structure. That is  $T_{DL}$  is originated from that spins tilt and generate a nonequilibrium out-of-plane spin polarization in response to an additional spin-orbit field during the acceleration of carries induced by the applied electric field. As described the above, the SOT-induced DL and FL spin torques are proportional to the strength of the electric field or electric current density. The SOT-induced spin torque,  $T_{ST}$ , can exert the magnetization dynamics modulation through the heterojunction.

Figures 5(a) and 5(b) show the typical rectifying voltage spectra of AMR and PHE measured at  $\theta_H = 0^\circ$  in the absence of the dc electric current. When the dc electric current was applied, the background voltage was too large to observe the rectifying AMR spectra. On the other hand, the rectifying PHE spectra could be measured as shown in Fig. 5(c), in which displays the magnified spectra in the red-colored dashed open squared area in Fig. 5(b) to magnify

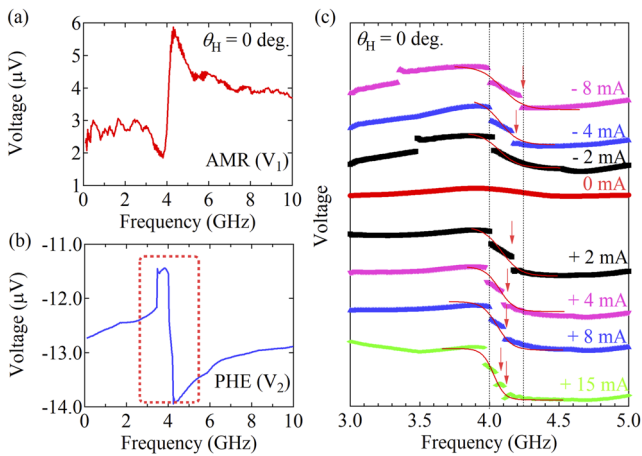


**FIG. 5.** Dc voltage spectra of (a) AMR and (b) PHE generated by the wire in response to the rf current only under the magnetic field of 100 G at  $\theta_H = 15^\circ$ . (c) The dc electric current dependence of PHE spectra of the magnified red dashed area in Fig. 5(b). Each PHE spectrum is vertically shifted for clarity.

the behaviors of spectra near the ferromagnetic resonance. The rectifying PHE voltage spectra with varying the dc electric current are vertically shifted and plotted for clarity as shown in Fig. 5(c). It can be clearly seen that the rectifying PHE spectra survives and strongly depends on the dc electric current. It can be seen that the spectral width of the ferromagnetic resonance, Full width at Half Maximum (FWHM), changes as the dc current is applied from  $-8$  mA (current density,  $j_{dc}$ , flowing through the electrode is  $-1.3 \times 10^{10}$  A/m<sup>2</sup>) to  $+15$  mA ( $j_{dc} = +2.5 \times 10^{10}$  A/m<sup>2</sup>). Each spectrum was measured after a time interval of about 3 min after dc current was applied, and the measurement was started only after a sufficient thermal equilibrium state was reached. Then, the contact resistance stabilized while confirming that the contact resistance had not changed. The discontinuous jumps in the spectra are probably due to magnetization dynamics induced by the dc current application.

Using the spectrum fitting function given by Eq. (3), all measured spectra were fitted as shown in Fig. 5(c). The red solid curves denote the fitting curves. As a result, we estimated the dc electric current dependence of resonance frequency and FWHM as

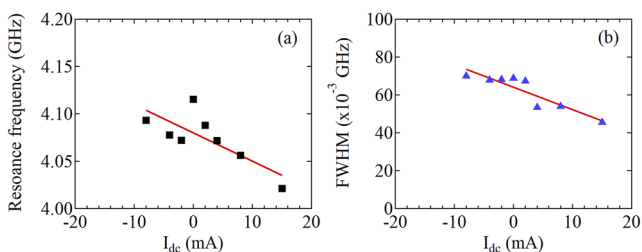


**FIG. 6.** The dc electric current dependence of (a) FMR frequency and (b) Full width at Half Maximum (FWHM).

shown in Figs. 6(a) and 6(b), respectively. Both linearly decrease with increasing the dc electric current. If the behavior is induced by the effect of Joule heat generation, the temperature rises in proportion to the square of the dc electric current. That is since the magnetization decreases in proportion to the square of the dc electric current, the resonance frequency simply decreases with the increase of dc electric current. At that time, the FWHM should be affected by the magnetization fluctuation due to the Joule heating, so it is expected that it will simply tend to increase. There is a minimum around the absence of dc electric current in the dc current dependence of resonance frequency. The dc electric current dependence of resonance frequency would indicate parabolic function. The behavior of FWHM also would exhibit the same way. However, the actual experimental results show a tendency that is completely different from this expectation. That is the results are not consisted with the scenario which the modulation of magnetization dynamics is induced by only the Joule heating effect. As a result, the results of Fig. 6 show that the dc current dependences of resonance frequency and FWHM varies linearly. The gradients are estimated to be  $\left| \frac{df_R}{dI} \right| = 4$  GHz/A and  $\left| \frac{d(\Delta f)}{dI} \right| = 1.8$  GHz/A, respectively. These behaviors are excited by the modulation of the magnetization due to the spin torque. Our study opens a new path to understand the quantitative evaluations for the contribution of SOT-induced spin torque in various systems.

In a system in which spin torque acts, it is possible to modulate magnetization dynamics. The changes of FWHM and resonance frequency by current or voltage can be quantitatively evaluated by the electrical rectifying ferromagnetic resonance measurements. As this study demonstrated, this measurement procedure can provide a useful method or tool for evaluating the contribution of SOT-induced spin torque. We remark here that it should also be possible to modulate magnetization dynamics by the SOT-induced spin torque in multilayer structures.

Our findings shed light on a new clue to control and modulate the magnetization dynamics in complex multilayer structures though the heterojunction among the heavy elemental electrodes, ferromagnetic and antiferromagnetic materials. We have shown that it is possible to modulate the magnetization dynamics without the need of a Zeeman field, which will be of potential importance in devices such as detectors, oscillators, magnetic random access memory, and magnetic logic devices.

## V. SUMMARY

In summary, we developed the automatic home-made measurement system to investigate the magnetization dynamics modulated by the SOT-FL spin torque using the rectifying PHE. Using the measurement system, we demonstrated experimentally that the modulation of magnetization dynamics in Py/NiO/Py wire deposited on Pt electrode is induced by the SOT-FL spin torque due to the dc electric current application in Pt layer. The rectifying PHE spectra can be strongly modulated by the application of dc electric current. We suggest that systematic studies of SOT-FL spin torque and estimation of Joule heating effects may additionally yield understanding of the phenomena and properties of multilayer systems. Our findings open venues for further studies on the

role of the heavy-metal electrode and evaluation of magnetization dynamics modulation induced by the SOT-FL spin torque in various systems.

## ACKNOWLEDGMENTS

We thank Professor Utsumi of University of Hyogo and Dr. Saiki of Hyogo Prefectural Institute of Technology for fruitful discussions and for providing experimental support. Funding: This work was supported in part by KRI Inc.

## AUTHOR DECLARATIONS

### Conflict of Interest

The authors have no conflicts to disclose.

## Author Contributions

**Akinobu Yamaguchi:** Conceptualization (lead); Data curation (lead); Formal analysis (lead); Funding acquisition (lead); Investigation (lead); Methodology (lead); Project administration (lead); Resources (lead); Software (lead); Writing – original draft (lead). **Nobuko Matsumoto:** Data curation (equal); Writing – original draft (equal). **Wataru Yoshikawa:** Data curation (equal); Writing – original draft (equal). **Yasuhisa Fujii:** Data curation (equal); Writing – original draft (equal).

## DATA AVAILABILITY

The data that support the findings of this study are available from the corresponding author upon reasonable request.

## REFERENCES

- B. Hillebrands and K. E. Ounadiela edit, *Spin Dynamics in Confined Magnetic Structures* (Springer, Berlin, Heidelberg, 2002), Vol. I–III.
- H. Zabel and S. D. Bader edit, *Magnetic Heterostructures—Advances and Perspectives in Spinstructure and Spintransport* (Springer-Verlag, Berlin Heidelberg, 2008).
- A. Yamaguchi, A. Hirohata, and B. Stadler edit, *Nanomagnetic Materials: Fabrication, Characterization and Application* (Elsevier, Amsterdam, 2021).
- J. C. Slonczewski, *J. Magn. Magn. Mater.* **159**, L1 (1996).
- L. Berger, *Phys. Rev. B* **54**, 9353 (1996).
- G. Tatara and H. Kohno, *Phys. Rev. Lett.* **92**, 086601 (2004).
- S. Zhang and Z. Li, *Phys. Rev. Lett.* **93**, 127204 (2004).
- A. Thiaville, Y. Nakatani, J. Miltat, and Y. Suzuki, *Europhys. Lett.* **69**, 990 (2005).
- A. Yamaguchi, T. Ono, S. Nasu, K. Miyake, K. Mibu, and T. Shinjo, *Phys. Rev. Lett.* **92**, 077205 (2004).
- N. Vernier, D. A. Allwood, D. Atkinson, M. D. Cooke, and R. P. Cowburn, *Europhys. Lett.* **65**, 526 (2004).
- C. K. Lim, T. Devolder, C. Chappert, J. Grollier, V. Cros, A. Vaurès, A. Fert, and G. Faini, *Appl. Phys. Lett.* **84**, 2820 (2004).
- M. Kläui, P.-O. Jubert, R. Allenspach, A. Bischof, J. A. C. Bland, G. Faini, U. Rüdiger, C. A. F. Vaz, L. Vila, and C. Vouille, *Phys. Rev. Lett.* **95**, 026601 (2005).
- M. Yamanouchi, D. Chiba, F. Matsukura, and H. Ohno, *Nature* **428**, 539 (2004).
- S. S. P. Parkin, M. Hayashi, and L. Thomas, *Science* **320**, 190 (2008).
- A. A. Tulapurkar, Y. Suzuki, A. Fukushima, H. Kubota, H. Maehara, K. Tsunekawa, D. D. Djayaprawira, N. Watanabe, and S. Yuasa, *Nature* **438**, 339 (2005).
- H. Kubota, A. Fukushima, K. Yakushiji, T. Nagahama, S. Yuasa, K. Ando, H. Maehara, Y. Nagamine, K. Tsunekawa, D. D. Djayaprawira, N. Watanabe, and Y. Suzuki, *Nat. Phys.* **4**, 37 (2007).
- J. C. Sankey, P. M. Braganca, A. G. F. Garcia, I. N. Krivorotov, R. A. Buhrman, and D. C. Ralph, *Phys. Rev. Lett.* **96**, 227601 (2006).
- J. C. Sankey, Y.-T. Cui, J. Z. Sun, J. C. Slonczewski, R. A. Buhrman, and D. C. Ralph, *Nat. Phys.* **4**, 67 (2007).
- S. Kanai, M. Yamanouchi, S. Ikeda, Y. Nakatani, F. Matsukura, and H. Ohno, *Appl. Phys. Lett.* **101**, 122403 (2012).
- T. Nozaki, Y. Shiota, S. Miwa, S. Murakami, F. Bonell, S. Ishibashi, H. Kubota, K. Yakushiji, T. Saruya, A. Fukushima, S. Yuasa, T. Shinjo, and Y. Suzuki, *Nat. Phys.* **8**, 491 (2012).
- L. Liu, T. Moriyama, D. C. Ralph, and R. A. Buhrman, *Phys. Rev. Lett.* **106**, 036601 (2011).
- S. D. Ganichev, E. L. Ivchenko, V. V. Bel'kov, S. A. Tarasenko, M. Sollinger, D. Weiss, W. Wegscheider, and W. Prettl, *Nature* **417**, 153 (2002).
- J. C. Rojas-Sánchez, L. Vila, G. Desfonds, S. Gambarelli, J. P. Attané, J. M. D. Teresa, C. Magén, and A. Fert, *Nat. Commun.* **4**, 2944 (2013).
- A. Manchon, H. C. Koo, J. Nitta, S. M. Frolov, and R. A. Duine, *Nat. Mater.* **14**, 871 (2015).
- H. Li, H. Gao, L. P. Zárbo, K. Výborný, X. Wang, I. Garate, F. Doğan, A. Čejchan, J. Sinova, T. Jungwirth, and A. Manchon, *Phys. Rev. B* **91**, 134402 (2015).
- D. Fang, H. Kurebayashi, J. Wunderlich, K. Výborný, L. P. Zárbo, R. P. Campion, A. Casiraghi, B. L. Gallagher, T. Jungwirth, and A. J. Ferguson, *Nat. Nanotechnol.* **6**, 413 (2011).
- L. Liu, C.-F. Pai, Y. Li, H. W. Tseng, D. C. Ralph, and R. A. Buhrman, *Science* **336**, 555 (2012).
- V. Scagnoli, U. Staub, Y. Bodenthin, R. A. de Souza, M. García-Fernández, M. Garganourakis, A. T. Boothroyd, D. Prabhakaran, and S. W. Lovesey, *Science* **332**, 696 (2011).
- T. Gao, A. Qaiumzadeh, H. An, A. Musha, Y. Kageyama, J. Shi, and K. Ando, *Phys. Rev. Lett.* **121**, 017202 (2018).
- W. L. Peng, J. Y. Zhang, G. N. Feng, X. L. Xu, C. Yang, Y. L. Jia, and G. H. Yu, *Appl. Phys. Lett.* **115**, 092402 (2019).
- R. Khymyn, I. Lisenkov, V. Tiberkevich, B. A. Ivanov, and A. Slavin, *Sci. Rep.* **7**, 43705 (2017).
- E. A. Mashkovich, K. A. Grishunin, R. M. Dubrovina, A. K. Zvezdin, R. V. Pisarev, and A. V. Kimel, *Science* **374**, 1608 (2021).
- T. Shang, Q. F. Zhan, H. L. Yang, Z. H. Zuo, Y. L. Xie, L. P. Liu, S. L. Zhang, Y. Zhang, H. H. Li, B. M. Wang, Y. H. Wu, S. Zhang, and R.-W. Li, *Appl. Phys. Lett.* **109**, 032410 (2016).
- J. Kim, J. Sinha, M. Hayashi, M. Yamanouchi, S. Fukami, T. Suzuki, S. Mitani, and H. Ohno, *Nat. Mater.* **12**, 240 (2012).
- C.-F. Pai, M.-H. Nguyen, C. Belvin, L. H. Vilela-Leão, D. C. Ralph, and R. A. Buhrman, *Appl. Phys. Lett.* **104**, 082407 (2014).
- C. O. Avci, K. Garello, M. Gabureac, A. Ghosh, A. Fuhrer, S. F. Alvarado, and P. Gambardella, *Phys. Rev. B* **90**, 224427 (2014).
- K.-S. Lee, D. Go, A. Manchon, P. M. Haney, M. D. Stiles, H.-W. Lee, and K.-J. Lee, *Phys. Rev. B* **91**, 144401 (2015).
- A. Yamaguchi, K. Motoi, H. Miyajima, T. Sato, and Y. Nakatani, *IEEE Trans. Magn.* **46**, 1994–1998 (2010); A. Yamaguchi, K. Motoi, H. Miyajima, A. Hirohata, T. Yamaoka, T. Uchiyama, and Y. Utsumi, *Appl. Phys. Lett.* **95**, 122506(1-3) (2009).
- A. Yamaguchi, K. Motoi, A. Hirohata, and H. Miyajima, *Phys. Rev. B* **79**, 224409 (2009); A. Yamaguchi, K. Motoi, A. Hirohata, H. Miyajima, Y. Miyashita, and Y. Sanada, *Phys. Rev. B* **78**, 104401(1-11) (2008).

- <sup>40</sup>Y. S. Gui, N. Mecking, X. Zhou, G. Williams, and C.-M. Hu, *Phys. Rev. Lett.* **98**, 107602 (2007); N. Mecking, Y. S. Gui, and C. M. Hu, *Phys. Rev. B* **76**, 224430 (2007).
- <sup>41</sup>M. Harder, Y. Gui, and C.-M. Hu, *Phys. Rep.* **661**, 1 (2016).
- <sup>42</sup>M. DC, R. Grassi, J. -Y. Chen, M. Jamali, D. R. Hickey, D. Zhang, Z. Zhao, H. Li, P. Quarterman, Y. Lv, M. Li, A. Manchon, K. A. Mkhoyan, T. Low, and J.-P. Wang, *Nat. Mater.* **17**, 800 (2018).
- <sup>43</sup>C. Safranski, E. A. Montoya, and I. N. Krivorotov, *Nat. Nanotechnol.* **14**, 27 (2019).
- <sup>44</sup>L. E. Dzyaloshinskii, *Sov. Phys. JIETP* **5**, 1259 (1957).
- <sup>45</sup>T. Moriya, *Phys. Rev.* **120**, 91 (1960).
- <sup>46</sup>A. Qaiumzadeh, R. A. Duine, and M. Titov, *Phys. Rev. B* **92**, 014402 (2015).